PHYSICAL REVIEW B VOLUME 43, NUMBER 3 15 JANUARY 1991-II

Electronic structure of strained-layer AlAs/InAs (001) superlattices

J. Arriaga
Instituto de Ciencia de Materiales, Consejo Superior de Investigaciones Cientificas Serrano, 123.28006 Madrid, Spain

G. Armelles
Centro Nacional de Microelectrónica, Consejo Superior de Investigaciones Cientificas Serrano, 144.28006 Madrid, Spain

M. C. Muñoz
Instituto de Ciencia de Materiales, Consejo Superior de Investigaciones Cientificas Serrano, 123.28006 Madrid, Spain

J. M. Rodríguez, P. Castrillo, and M. Recio
Centro Nacional de Microelectrónica, Consejo Superior de Investigaciones Cientificas Serrano, 144.28006 Madrid, Spain

V. R. Velasco
Instituto de Ciencia de Materiales, Consejo Superior de Investigaciones Cientificas Serrano, 123.28006 Madrid, Spain

F. Briones
Centro Nacional de Microelectrónica, Consejo Superior de Investigaciones Cientificas Serrano, 144.28006 Madrid, Spain

F. García-Moliner
Instituto de Ciencia de Materiales, Consejo Superior de Investigaciones Cientificas Serrano, 123.28006 Madrid, Spain
(Received 26 July 1990)

(001) superlattices containing 15 principal layers of AlAs and either one or two of InAs have been grown by atomic-layer molecular-beam epitaxy on undoped (001) GaAs substrates. The samples, between 0.1 and 0.3 μm thick, have been studied by photoluminescence, electroreflectance, and piezoreflectance and monitored by phonon Raman-scattering spectroscopy and x-ray diffractometry. An empirical tight-binding model, combined with surface Green-function matching, is used to discuss the experimental data. An overall picture is obtained for the electronic structure of these superlattices with a valence-band offset close to 0.5 eV, which is consistent with the observed spectra.

I. INTRODUCTION

The numerous device applications of semiconductor superlattices have stimulated a great deal of interest in their fundamental physical properties. Strained-layer superlattices (SL's) have the additional attraction of enlarging the scope of potential applications, on account of the profound influence that built-in strains have on the resulting electronic structure, particularly for states near the band gap. This determines a rich phenomenological variety which makes strained-layer systems very useful.[1,2] Also, short period SL's built from akin binary compounds can exhibit a more regular behavior than the corresponding ternary alloys, due to the absence of compositional fluctuations. Among the outstanding properties of strained-layer SL's is the possibility of modeling in a certain range the structure of the valence bands, the achievement of higher carrier mobilities, and the effectiveness of buffering the growth.

The practical disadvantage of strained-layer systems is that they are, in general, rather difficult to grow satisfactorily and relatively less is known compared with the abundance of information available on systems made of compounds with good lattice matching. However, recent developments in conventional growth techniques, such as atomic-layer molecular-beam epitaxy, migration-enhanced epitaxy, and metal-organic chemical-vapor deposition, among others, make it possible to obtain fairly good specimens for thicknesses of the constituent layers below some characteristic critical values.[3,4] The knowledge of the electronic structure of such heterostructures should constitute the basis for further developments in this field.

Although there have been some reports on GaAs/InAs and AlAs/InAs SL's, these generally focus on the growth problems and crystalline quality of the epitaxial layers,[5,6] while their electronic structures are poorly known, especially in the case of AlAs/InAs, for which no information on the band offset appears to be available.

The purpose of this paper is to present some experimental and theoretical studies of AlAs/InAs (001) SL's aimed at obtaining some information on their electronic structure. We shall concentrate on the (15,1) and (15,2) SL's, which are the ones experimentally accessible with acceptable quality. The thicker layer (15 principal layers) is always, of course, that of AlAs. Due to the thinness of the InAs layers, the use of an empirical tight-binding (ETB) Hamiltonian, on which our calculations will rest,

 ©1991 The American Physical Society

is really at its limit and no accurate quantitative reliance can be expected. However, its simplicity allows for a flexible study of possible different alternatives and effects and, combined with experimental evidence, one can narrow the range of options within plausible limits that do provide reasonable information on the electronic properties of these SL's.

Section II describes the model and the technique employed in the theoretical calculations, while Secs. III and IV present the experimental results together with the proposed theoretical interpretation with which, within reasonable limits, as explained, some information can be surmised on their electronic structure.

II. THEORETICAL MODEL

We used an ETB Hamiltonian with an sp^3s^* orbital basis,[7] including spin-orbit splitting.[8] After a two-dimensional Fourier transform in the plane of the interfaces this amounts to ten layer orbitals per atomic layer. With two atomic layers per *principal layer*[9] we have a total of 20 layer orbitals per principal layer—henceforth simply denoted as layer. This is the order of the matrices involved in the layer description of each constituent material. Inclusion of strain is an important element in the calculation. This modifies the interatomic distances and bond angles. In an ETB model this results in modifications of the angular dependence of the structure factors[10] and of the nondiagonal Hamiltonian parameters, which are usually evaluated by a scaling formula of the type[11]

$$H_{\alpha\beta}(d)=H_{\alpha\beta}(d_0)(d/d_0)^{-\nu} , \qquad (2.1)$$

where α,β are atomic orbitals, d_0/d is the unstrained divided by the strained interatomic distance, and ν differs, and may or may not depend on $(\alpha\beta)$, according to different scaling rules. For sp^3s^* nearest-neighbor parametrization Harrison's rule is $\nu=2$ for all matix elements.[11,12] This often works rather well. Other exponents have been used[13] for strained Si/Ge SL's. A more elaborate model has been recently proposed[14] for ionic semiconductors in which $\nu_{ss}=3.7$, while Harrison's rule is used for the rest. This appears to provide a better fit to the band-gap variation under pressure in III-V compounds. We have used both schemes[12,14] in the present calculations and found that the difference in energy position of the resulting band-edge levels is of the order of the experimental accuracy.

The calculations were performed by using the surface Green-function matching (SGFM) method which has been explained in detail elsewhere.[15,16] In this method one evaluates the Green function of the superlattice as a function of energy E, two-dimensional in-plane wavevector $\mathbf{k}$, one-dimensional (super) wave vector q in the growth direction, and layer indices n,n'. From this one can obtain the energy eigenvalues $E_j(\mathbf{k},q)$, where j labels the subbands of the SL, and the spectral functions of interest. In particular, for each eigenstate one can calculate the spatial dependence of the spectral strength or local density of states (LDOS). In a tight-binding model this corresponds to the discrete-valued squared amplitude as a function of layer index n. It is furthermore possible to separate out the LDOS in the anion and cation layers, and also the contributions from the different layer orbital components having (s, p_x, p_y, p_z, or s^*)-like characters as will be seen later. In correspondence with the optical experiments to be described in Sec. III, we have performed all calculations for $k=q=0$, i.e., for the Γ point of the SL.

TABLE I. Empirical matrix elements of the sp^3s^* Hamiltonian in eV, including the spin-orbit splitting.

	AlAs	InAs
$E(s,a)$	-7.5250	-9.5381
$E(p,a)$	0.9400	0.7733
$E(s^*,a)$	7.4830	7.2730
$E(s,c)$	-1.1650	-2.7219
$E(p,c)$	3.5400	3.5834
$E(s^*,c)$	6.7270	6.6095
$V(s,s)$	-6.6640	-5.6052
$V(x,x)$	1.9320	1.8398
$V(x,y)$	4.2440	4.3977
$V(sa,pc)$	5.1040	3.0205
$V(sc,pa)$	5.4760	5.3894
$V(s^*a,pc)$	4.4920	3.2191
$V(s^*c,pa)$	4.9960	3.7234
λ_a	0.1385	0.1385
λ_c	0.0080	0.1290

The SGFM method can be used for any number of layers of each constituent material, even down to only one, as has been demonstrated in the study of graphite intercalation compounds.[17] The difficulty with the extreme case, the (15,1) SL, is not with the technique but with the model. One has to invoke some parameter related to the relative level alignment, which by tradition we shall continue to refer to as the *band offset*, although one cannot take this literally in this case. We shall introduce, in this sense, the valence-band offset ΔE_v, which we shall measure from the top of the AlAs valence band (VB). In the absence of any indication about ΔE_v we shall take this as an adjustable parameter. In fact one of the purposes of the present work is to obtain a plausible estimate of ΔE_v. The other input parameters used in the calculations to describe the unstrained constituent semiconductors, are listed in Table I.

III. EXPERIMENTAL RESULTS

The samples, between 0.1 and 0.3 μm thick, were grown by atomic-layer molecular-beam epitaxy on undoped (001) GaAs substrates. The In and Al fluxes were previously adjusted by means of reflection high-energy-electron-diffraction specular beam oscillations to yield a growth rate of one monolayer per second. More details on the growth procedure have been reported elsewhere.[18] The SL's were further characterized by x-ray diffractometry. A double-crystal x-ray diffractometer was used and the scans were recorded near (004) and (115) reflections of the GaAs substrate in order to obtain the

TABLE II. In-plane ($a_{\parallel}$) and average perpendicular ($a_{\perp}$) lattice constant obtained for the superlattices by x-ray diffractometry for different sample thicknesses. Samples 1 and 2 correspond to the nominally (15,1) SL's, whereas 3 and 4 correspond to the (15,2) SL's.

Sample	Thickness (μm)	$a_{\parallel}$ (Å)	$a_{\perp}$ (Å)
1	0.1	5.654	5.704
2	0.3	5.662	5.713
3	0.1	5.657	5.750
4	0.3	5.691	5.742

in-plane ($a_{\parallel}$) and average perpendicular ($a_{\perp}$) lattice parameters of the SL. These are given in Table II. The x-ray results indicate that the strain is confined to the InAs layers, which are under 7% biaxial compression, while the AlAs layers remain unstrained. Then, the resulting lattice parameters, on which the calculations rests are as follows: the SL in-plane $a_{\parallel}$ is equal to that of the unstrained AlAs layers while $a_{\perp}$ is evaluated from standard elasticity theory in terms of the bulk rigidity moduli C_{12} and C_{11}.

The samples were studied by low-temperature (~ 10 K) photoluminescence (PL), room-temperature piezoreflectance (PZR), and electroreflectance (ER) at various temperatures. Complementary Raman-scattering (RS) measurements were also carried out. Figure 1 shows PL

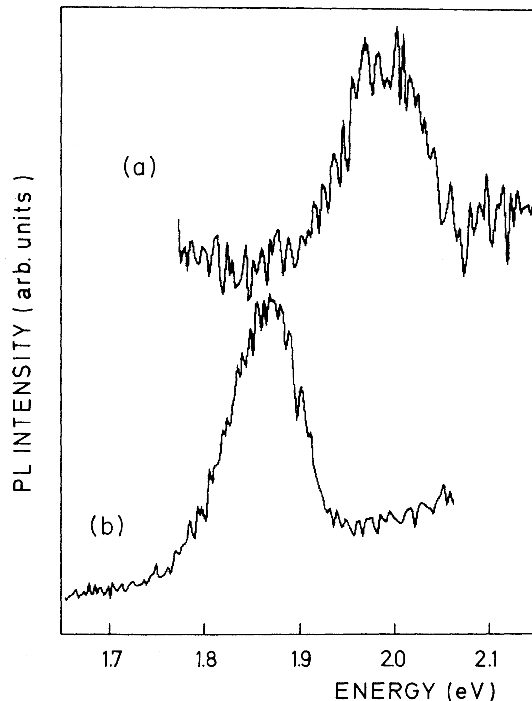

FIG. 1. PL spectra at ~ 10 K: (a) sample 1 and (b) sample 3.

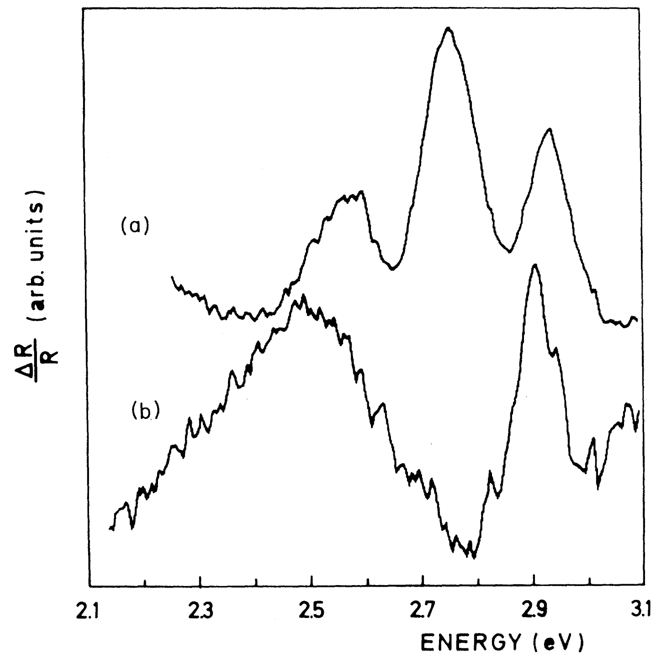

FIG. 2. Room-temperature PZR spectra for the SL's of Fig. 1: (a) sample 1 and (b) sample 3.

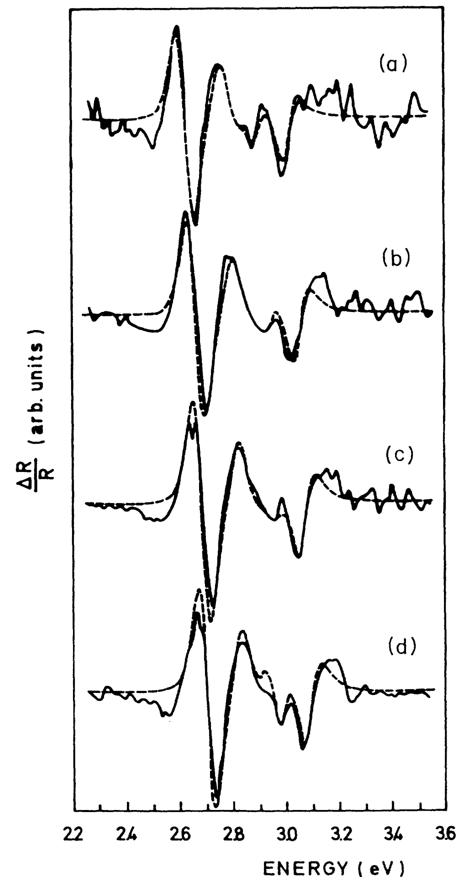

FIG. 3. ER spectra taken at different temperatures for sample 1: (a) 290 K, (b) 220 K, (c) 170, and (d) 120 K.

spectra for the (15,1) and (15,2) SL's. In both cases a broad peak at energies below the AlAs indirect gap is observed and the peak of the (15,2) SL appears at a lower energy than that of the (15,1).

The PZR spectra are shown in Fig. 2. Three and two peaks are observed for the (15,1) and (15,2) SL's, respectively. In both spectra the peak at the highest energy corresponds to the E_1 transition of the bulk GaAs substrate. ER spectra were also obtained at various temperatures. Four of them for the (15,1) SL are shown in Fig. 3. There is a relatively broad feature in the energy range at which the two lower PZR peaks are observed, and a less intense structure appears at higher energy. We estimate that these data correspond to the low-field regime and on this basis we have tried to fit the experimental spectra with the third derivative functional form[19] in terms of four transitions: two of them corresponding to the two transitions observed with PZR, another one at a higher energy (3.00 eV), and a fourth one, at 2.89 eV, which is the E_1 transition of the bulk GaAs substrate. The fit, dashed line in Fig. 3, is reasonably good. The ER spectra obtained for the (15,2) SL were more complicated and the identification of neat transition energies from them is somewhat less clear. Table III summarizes the transition energies obtained with the different techniques. Now, the same electronic transitions can be part of phonon Raman-scattering events. The optical phonons of either InAs or AlAs are confined in each one of these materials, as their dispersion curves do not overlap in frequency. Therefore, Raman spectroscopy can be used to probe the spatial confinement of the transitions described above, by following the intensity ratio of the phonons of both materials. The InAs to AlAs ratio increases as we approach the 2.6 and 2.75 eV transition on the (15,1) SL and the 2.5-eV transition on the (15,2) SL, the increase being larger for the latter. This can be clearly appreciated in Fig. 4, which shows Raman spectra for exciting wavelengths near and away from resonance.

TABLE III. Experimental transition energies in eV, obtained by different methods as indicated.

Sample	PL (10 K)	PZR (RT)	ER (RT)
1	1.98	2.6,2.75	2.6,2.75,3.00
3	1.87	2.5	

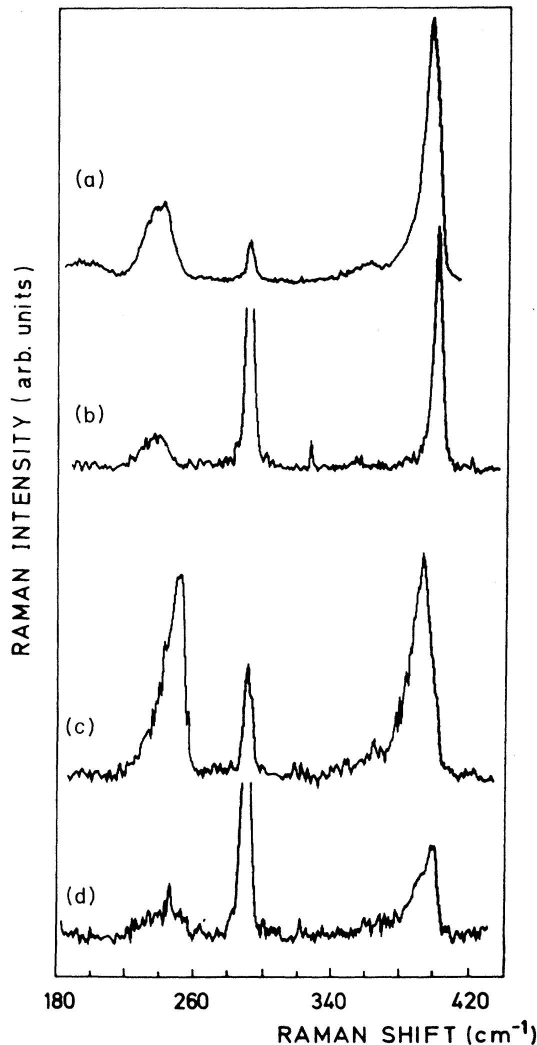

FIG. 4. Room-temperature Raman spectra obtained near [(a) and (b)] and outside [(c) and (d)] resonance for samples 1 [(a) and (c)] and 3 [(b) and (d)].

IV. DISCUSSION

It is very useful to have alternative experimental results for the same samples. As explained above, one could hardly obtain an unambiguous picture for any single technique, but the various data provide complementary information which allows one to discard options and narrow down the range of possible conclusions.

Given the ease with which theoretical calculations can be performed we can follow not only the spatial confinement of the electronic states involved in the proposed transitions but also, and specially, their predominant orbital character. With this we can finally obtain a plausible picture.

Tables IV and V show the most significant energy values near the band edges of the (15,1) and (15,2) SL's, respectively, calculated at the Γ point of the SL in the manner described in Sec. II. A few specifications are in order. (i) For each case the calculation was done by using the two exponents ($\nu_{ss}=2$ and 3.7) corresponding to the two scaling rules mentioned in Sec. II. This leaves the valence band unaltered and results in very small changes in the conduction band. (ii) The valence-band offset ΔE_v is, as discussed above, a trial parameter which fixes the relative level alignments. In our calculation this is done *before* strain is introduced. The zero energy is at the top of the VB of *unstrained* AlAs. The top of the VB of unstrained InAs is fixed at an energy ΔE_v above the reference level. Then the effects of mismatch and stress are in-

troduced and the resulting eigenvalues and discrete-valued amplitudes for the SL states are calculated. Without strain one would expect the upper VB states of the SL states to be all below the top of the well material, i.e., at energies $<\Delta E_v$. However, after the effects of stress are introduced this need not be necessarily so. Thus one can understand that for $\Delta E_v=0$ two levels appear with $E\geq 0$. (iii) The tables also give the dominant orbital character and the material in which the amplitude is mainly confined. As discussed in Sec. II, this was calculated as the LDOS or local spectra strength, which corresponds to the squared amplitude of the state under study. (iv) Due to folding effects many more energy levels usually appear in a given energy range. These have been sorted out and only those are given which may be relevant for the interpretation of the observed transition.

The two highest VB states, for the range of ΔE_v presented in the tables, are always confined to InAs, in agreement with the results of Raman spectroscopy and have uniform orbital character, with p_x and p_y characters equally dominant for both and p_z character also for the V_2 state. On the contrary, these features differ for the three lowest conduction-band (CB) states and are more sensitive to the number n of InAs layers. The relative ordering of their eigenvalues depends on n and also on the assumed value of ΔE_v, a feature which helps to bracket this between plausible limits.

In attempting to correlate these results with the observed transitions we must discuss simultaneously the information contained in Tables III–V. Let us concentrate on the (15,1) SL, for which the experimental results are neater due to their better crystalline quality. The lowest observed transition, at 1.98 eV appears only in PL and not in PZR or ER. For $\Delta E_v > 0.2$ eV the lowest CB state has predominant p_z character and is confined to AlAs—Table IV and Figs. 5 and 6. Since the highest VB state is confined to InAs and has p_x and p_y character—Figs. 5 and 6—for ΔE_v greater than 0.2 eV one expects the lowest transition to appear in PL only, and not in PZR or ER. This does agree with experimental evidence and sug-

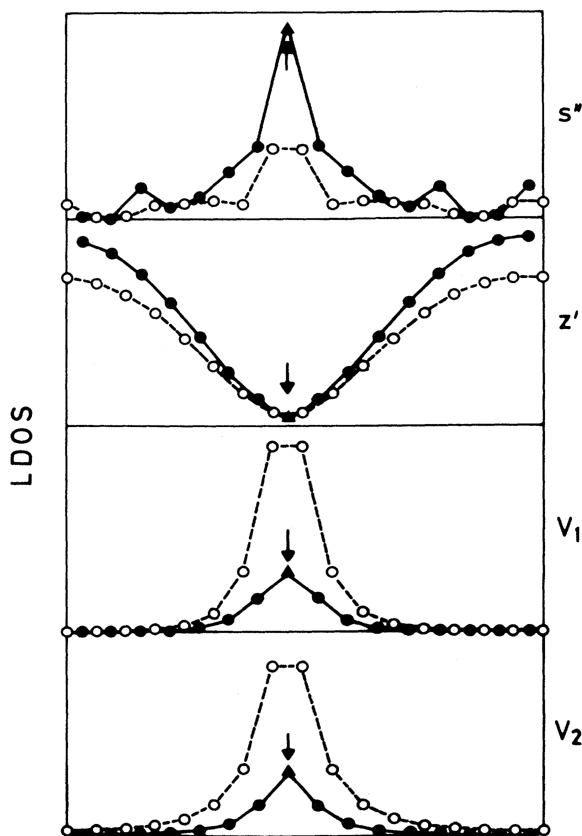

FIG. 5. The spatial distribution of the spectral strength for a (15,1) SL with $\Delta E_v=0.5$ eV and $v_{ss}=3.7$, for the states listed in Table IV. ○, As; ●, Al; and ▲, In layers, the vertical arrow marks the In layer.

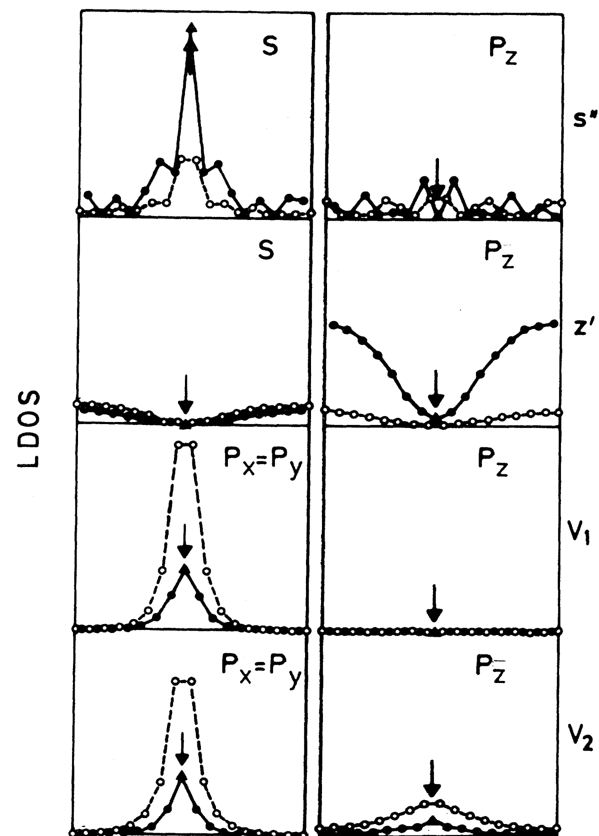

FIG. 6. The spatial distribution of the contribution of the different orbitals to the spectral strength of the states of the (15,1) SL shown in Fig. 5.

gests 0.2 eV as a lower bound for ΔE_v. We may associate the observed PL peak with the transition $V_1 - z'$, even if it were associated with a defect, which is possible.

The actual estimated value for the energy of this transition decreases as the assumed value of ΔE_v increases and is insensitive to the scaling rule. For $0.4 \leq \Delta E_v \leq 0.8$ eV the transition energy ranges from 2.04 to 1.80 eV, in the neighborhood of the experimental value 1.98 eV. This suggest something like 0.8 eV as an upper bound for ΔE_v.

Now consider the two lowest transitions, 0.15 eV apart, seen in PZR and ER spectra. These transitions involve photon absorption, and they should be from the two highest VB levels to a CB state with s character and confined in the InAs layer. This is the case for the s'' state, for which we note (i) that it depends rather more strongly on ΔE_v and (ii) that it does depend on the exponent ν_{ss}. The energy difference (0.15 eV) between these two transitions should then be due to the energy difference between V_1 and V_2 states, the transitions being identified as V_1-s'' and V_2-s''. We now must account for the energies of these two transitions and their difference simultaneously. This leads us as the most likely combination to the value $\Delta E_v = 0.5$.

Figures 5 and 6 display the spatial distribution of s'', z', V_1, and V_2 of the (15,1) SL for $\Delta E_v = 0.5$ eV. The total strength is given in Fig. 5, while in Fig. 6 this is decomposed into the different orbital components. Note the strong confinement of the s'', V_1, and V_2 states about the In layer, especially in the case of V_1 and V_2. Their dominant orbital symmetry is that of the heavy- and light-hole states, respectively, of bulk InAs; since the SL is grown in the z direction, the SL unit cell remains tetragonal under biaxial compression of one of their constituents and the symmetry of these states remains unaltered.

Folding effects are very important in the CB, where

TABLE IV. Calculated energy levels in eV, measured from the AlAs VB edge, of the most significant states near the band edges of the (15,1) superlattice. Top: CB with Harrison's scaling rule (all $\nu = 2$). The state labeled m, and denoted by an asterisk, has mixed orbital character (mainly, s^* and p_z) and has amplitude in both materials, while z' denotes predominant p_z character with spatial confinement in AlAs and s'' predominant s character, with spatial confinement in InAs. Middle: Same as top with a different scaling rule, $\nu_{ss} = 3.7$. Bottom: The two highest VB states, denoted V_1 and V_2. Both have equal spectra strength of p_x and p_y orbital character and spatial confinement about the InAs layer the V_2 state has also p_z. For discussion and interpretation see text.

	0.0	0.2	0.4	0.5	0.6	0.8	1.0
CB							2.88:s''
d^{-2}						2.84:s''	
					2.72:s''		
				2.67:s''			
			2.63:s''				
		2.53:s''					
	2.36:s''		*2.33:m	*2.34:m	*2.35:m	*2.33:m	*2.33:m
	2.28:z'	2.29:z'	2.27:z'	2.27:z'	2.28:z'	2.28:z'	2.28:z'
		*2.25:m					
	*2.19:m						
CB							2.90:s''
d^{-37}						2.87:s''	
				2.72:s''	2.75:s''		
			2.67:s''				
		2.57:s''					
2.	2.42:s''						
			*2.33:m	*2.34:m	*2.35:m	*2.33:m	*2.33:m
	2.27:z'	2.29:z'	2.27:z'	2.27:z'	2.28:z'	2.28:z'	2.28:z'
		*2.25:m					
	*2.19:m						
VB							0.63:V_1
						0.48:V_1	0.46:V_2
					0.35:V_1	0.32:V_2	
				0.29:V_1			
			0.23:V_1				
					0.20:V_2		
		0.13:V_1		0.14:V_2			
			0.10:V_2				
	0.05:V_1						
	0.00:V_2	0.03:V_2					

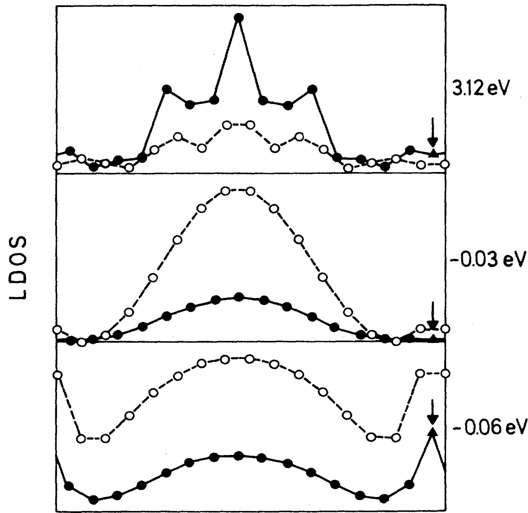

FIG. 7. The spatial distribution of the spectral strength for the AlAs barrier states of a (15,1) SL with $\Delta E_v = 0.5$ eV and $v_{ss} = 3.7$. See text.

they even determine the spatial character of the SL states. The lowest one z' is confined in the AlAs layers and has predominant p_z orbital character. This may have its origin in the lowest CB state at the X point of bulk AlAs, which after folding becomes a Γ point of the SL while maintaining its orbital character. Just above this level there are several CB energy levels all with the same orbital character and spatial confinement, which can be ruled out as final states for absorption transitions (PZR and ER), until we find the s'' state which we have associated with the two absorption transitions, as explained above.

A third peak appears in ER at 3.00 eV. The interpretation of this peak is more difficult. Due to the evolution of CB and VB energy levels there is a bunching up of possible transition energies in a narrow interval and any assignment is somewhat ambiguous. With due reservations and after similar considerations of orbital character and spatial confinement we find as the most plausible conclusion that this may be the transition from either of the two VB states at -0.03 and -0.06 eV to the CB state at 3.12 eV described in Fig. 7, which corresponds to AlAs barrier levels. Note that here the vertical arrow corre-

TABLE V. Same as Table IV but for the (15,2) superlattice.

	0.0	0.2	0.4	0.5	0.6	0.8	1.0
CB							2.46:s''
d^{-2}	*2.36:m	*2.34:m	*2.35:m	*2.35:m	*2.35:m	*2.35:m	*2.36:m
						2.34:s''	
	2.27:z'	2.27:z'	2.27:z'	2.27:z'	2.27:z'	2.27:z'	2.27:z'
					2.20:s''		
				2.14:s''			
			2.07:s''				
		1.94:s''					
	1.80:s''						
CB							2.54:s''
$d^{-3.7}$	*2.36:m	*2.34:m	*2.35:m	*2.36:m	*2.36:m	*2.36:m	*2.36:m
						2.35:s''	
	2.27:z'	2.27:z'	2.27:z'	2.27:z'	2.27:z'	2.27:z'	2.27:z'
					2.25:s''		
				2.21:s''			
			2.14:s''				
		2.01:s''					
	1.86:s''						
VB							0.53:V_1
						0.42:V_1	
					0.32:V_1		0.34:V_2
				0.27:V_1			
			0.23:V_1			0.23:V_2	
		0.16:V_1			0.14:V_2		
			0.07:V_2	0.10:V_2			
	0.01:V_1	0.03:V_2					
	0.00:V_2						

sponding to the In layer is at the edge of the figure. The CB state is mainly s like and is confined in the AlAs layers. The two valence-band states have predominant p_x and p_y orbital character and originate from the bulk AlAs heavy- and light-hole states. The stronger confinement of the hh-like state may be due to its heavier effective mass. Then, for the (15,1) SL the calculations explain altogether the experimental results, although there is a general tendency to underestimate the transition energies.

The experimental results for the (15,2) SL are very similar to those obtained for the (15,1) case, with a tendency for all transitions to appear at slightly lower energies. Table V shows the main theoretical results for the (15,2) SL. The general discussion, based on spatial confinement and orbital character, is as before and need not be repeated. On comparing with the (15,1) case the tendency is for the transition energies to be smaller, in qualitative agreement with experimental observation. However, for $\Delta E_v \leq 0.6$ eV, the lowest CB state with predominant s character is confined in the InAs layers and therefore it should be observed in all PL, PZR and ER, against experimental evidence. Furthermore, for $\Delta E_v > 0.6$ eV, when the lowest CB state is of the z' type, the actual estimated values for the energies of the transitions V_1-s'' and V_2-s'' are about 0.6 eV lower than the experimental values. Altogether a quantitative fit is harder to obtain in this case, which may be due to the comparatively worse crystalline quality of the sample.

Moreover, some discrepancies between theory and experiment are expected due to the use of standard bulk elasticity which may not be fully warranted.[20] For a try we have calculated the energy levels of the (15,1) and (15,2) SL's keeping $a_\perp$ in the InAs layers unstressed. The transition energies associated with the experimental spectra for $\Delta E_v = 0.5$ eV and $v_{ss} = 3.7$ are given in Table VI. Now the general features are the same for both the (15,1) and (15,2) SL's in agreement with experiments. On comparing with the values obtained from Tables IV and V there are two significative facts. (i) All the transition energies increase drastically and (ii) for the (15,2) SL the lowest conduction-band state becomes p_z-like and AlAs confined. Then, with $a_\perp$ for InAs evaluated from bulk elasticity we underestimate the observed transition energies, while with this parameter unchanged we overestimate them. It is not unlikely that the actual value of $a_\perp$ (InAs) may be somewhat in between. In addition, some In segregation in the AlAs layer[21] may also account for the experimental and theoretical differences. Calculations performed with a somewhat diffuse profile of In concentration change the transition energies in the direction of the experimental findings.

TABLE VI. Theoretical transition energies for the (15,1) and (15,2) SL's calculated with $\Delta E_v = 0.5$ eV and $\Delta a_\perp$ (InAs)$=0.0$.

	(15,1)	(15,2)
V_1-z'	2.10	2.14
V_1-s''	2.74	2.45
V_2-s''	2.83	2.54

In conclusion, although we could not at this stage claim to precise quantitative accuracy, we do obtain a quite plausible picture of the electronic structure of strained AlAs/InAs superlattices, compatible with the scaling law $v_{ss} = 3.7$ and with $\Delta E_v \simeq 0.5$ eV as a suggested estimate of the band offset.

ACKNOWLEDGMENTS

This work was partly supported by the Spanish Comision Interministerial de Ciencia y Tecnología under Grant No. MAT88-0547. One of the authors, J. Arriaga, is indebted to Consejo Nacional de Ciencia y Tecnológia (CONACYT) (México) for support. We are very grateful to J. P. Silveira and M. Vázquez of the Centro Nacional de Microelectrónica for growing the samples.

[1] G. C. Osbourn, IEEE Quantum Electron. **QE-22**, 1677 (1986).
[2] D. L. Smith and C. Mailhiot, Rev. Mod. Phys. **62**, 173 (1990).
[3] F. Briones, L. González, and A. Ruiz, Appl. Phys. A **49**, 729 (1989).
[4] *Compound Semiconductor Strained-layer Superlattices,* edited by R. M. Biefeld (Trans Tech, Aedermannsdorf, Switzerland, 1989).
[5] K. Nishi, T. Anan, Y. Ide, and K. Onabe, J. Cryst. Growth, **95**, 202 (1989).
[6] J. M. Gerard (unpublished).
[7] P. Vogl, H. P. Hjalmarson, and J. D. Dow, J. Phys. Chem. Solids **44**, 365 (1983).
[8] N. J. Chadi, Phys. Rev. B **16**, 790 (1977).
[9] M. C. Muñoz, V. R. Velasco, and F. García-Moliner, Phys. Scr. **35**, 504 (1987).
[10] W. Pötz and P. Vogl, Phys. Rev. B **24**, 2025 (1982).
[11] W. A. Harrison, *Electronic Structure and the Properties of Solids* (Freeman, San Francisco, 1980).
[12] S. Y. Ren and W. A. Harrison, Phys. Rev. B **23**, 762 (1982); W. A. Harrison, *ibid.* **24**, 5835 (1981).
[13] L. Brey and C. Tejedor, Phys. Rev. Lett. **59**, 1022 (1987).
[14] C. Priester, G. Allan, and M. Lannoo, Phys. Rev. B **37**, 8519 (1988).
[15] F. García-Moliner and V. R. Velasco, *Progress in Surface Science,* edited by S. G. Davidson (Academic, New York, 1986), Vol. 21, p. 93.
[16] M. C. Muñoz, V. R. Velasco, and F. García-Moliner, Phys. Rev. B **39**, 1786 (1989).
[17] V. R. Velasco, F. García-Moliner, L. Miglio, and L. Colombo, Phys. Rev. B **38**, 3172 (1988).
[18] M. Vázquez, J. P. Silveira, L. González, M. Pérez, G. Armelles, J. L. de Miguel, and F. Briones, J. Cryst. Growth **102**, 4 (1990).
[19] D. E. Aspnes and V. E. Rowe, Phys. Rev. B **5**, 4022 (1972).
[20] H. Oyanagi, Y. Takeda, T. Matsushita, T. Ishiguro, T. Yao, and A. Sasaki, Superlatt. Microstruct. **4**, 413 (1988).
[21] J. M. Moison, C. Guille, F. Houzay, F. Barthe, and M. van Rompay, Phys. Rev. B **40**, 6149 (1989).